A Novel Method for Studying the Dynamics of Confined Polymers in Nanoparticles in Nanoblends

ARTICLE *in* MACROMOLECULES · JANUARY 2010

Impact Factor: 5.8 · DOI: 10.1021/ma802734j · Source: OAI

Macromolecules

Subscriber access provided by UNIV JOSEPH FOURIER GRENOBLE

Article

A Novel Method for Studying the Dynamics of Polymers Confined in Spherical Nanoparticles in Nanoblends

Mohamed Yousfi, Lionel Porcar, Peter Lindner, Franc#ois Boue#, and Yahya Rharbi

Macromolecules, **Article ASAP** • Publication Date (Web): 24 February 2009

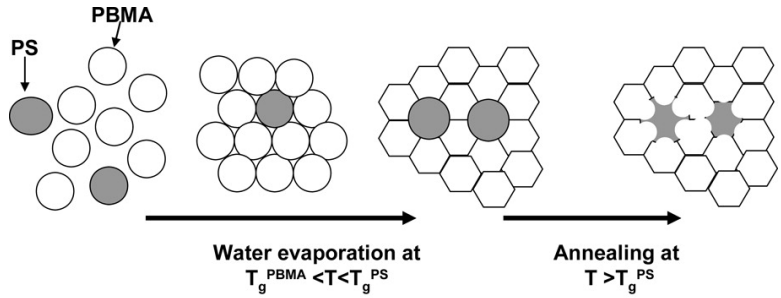

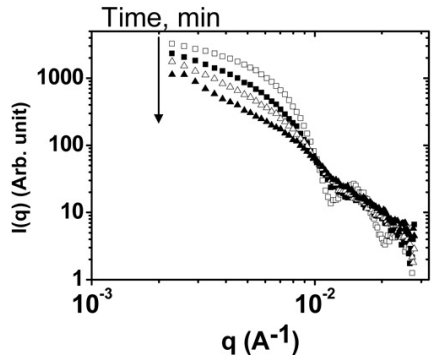

More About This Article

Additional resources and features associated with this article are available within the HTML version:

- Supporting Information
- Access to high resolution figures
- Links to articles and content related to this article
- Copyright permission to reproduce figures and/or text from this article

View the Full Text HTML

Macromolecules is published by the American Chemical Society. 1155 Sixteenth Street N.W., Washington, DC 20036

A Novel Method for Studying the Dynamics of Polymers Confined in Spherical Nanoparticles in Nanoblends

Mohamed Yousfi,[†] Lionel Porcar,[‡] Peter Lindner,[‡] François Boué,[§] and Yahya Rharbi*,[†]

Laboratoire de Rheologie, UJF/INPG/CNRS, BP 53, Domaine universitaire 38041, Grenoble, France, Institut Laué-Langevin, BP 156 38042, Grenoble, France, and Laboratoire Léon Brillouin, CEA Saclay, 91191 Gif-sur-Yvette, France

Received December 7, 2008; Revised Manuscript Received January 22, 2009

ABSTRACT: The advances in new technologies have prompted the need for functional systems smaller than the gyration radius of polymer chains. Thus, understanding how nanoconfinement affects polymer properties has been the focus of a lot of research for over a decade. Polystyrene in particular has been reported to be strongly affected when nanoconfined as a thin film and specifically its glass transition temperature (T_g) is reported to decrease with decreasing film thickness. Tremendous effort has been dedicated to developing methods for quantifying the large-scale dynamic of nanoconfined polymers: film dewetting, film contraction, nanobubble inflation, nanoparticle imbedding and healing of deformed surfaces etc. In this work we describe a novel method to study the large scale dynamic and nanomechanical properties of nanoconfined polymers in nanoparticles in nanoblends. Nanoblends of dPS/PBMA were prepared from a mixture of colloidal suspensions of cross-linked PBMA and traces of dPS nanoparticles via water evaporation. The polymer blends were prepared at temperatures well below the glass transition of PS (T_g^{PS}) and above the T_g of cross-linked PBMA particles (T_g^{PBMA}). In these conditions we expect the PBMA particles to deform under capillary pressure to fill the interstices between them and the glassy PS nanoparticles to remain spherical. During the preparation of the nanoblends the elastic energy is stored within the deformed cross-linked PBMA nanoparticles. Upon annealing the films above T_g^{PS}, the PBMA nanoparticles regain their spherical shape and release the stored elastic energy, which induces the deformation of the PS nanoparticles. Small angle neutron scattering is then used to monitor the shape evolution of the PS nanoparticles and to quantify the relaxation dynamics of the polystyrene nanoparticles.

1. Introduction

Advances in new technologies have prompted the need for functional systems smaller than the gyration radius of polymer chains. This is why understanding how nanoconfinement affects polymer properties has been the focus of a lot of research for over a decade.[1−21] In particular, the nanoconfined glass transition (T_g) of polymer thin films has been extensively studied[1−11] on both supported and free-standing films using various experimental techniques; Brillouin light scattering,[2] ellipsometry,[3,5] dielectric relaxation[4] and fluorescence.[7] For example, these reports substantially agreed that the T_g of polystyrene (PS) decreases with decreasing film thickness h for $h < 50$ nm. They demonstrate the relevance of polymer structure and polymer/substrate interactions in confined T_g. However, how nanoconfinement affects polymer dynamics and the nanomechanical properties is not yet fully understood. The reduction of nanoconfined T_g in polystyrene with decreasing film thickness infers the presence of a surface polymer layer with higher mobility than the bulk.[7,10] The short scale dynamic of polymer thin film has mainly been investigated using the dielectric relaxation technique.[4] On the other hand, various methods have been proposed to quantify the large-scale dynamic of nanoconfined polymers. Reiter et al.[12] used the dynamic of dewetting of polystyrene from substrate to extract information on the dynamics of polymer chains. Dutcher et al. also investigated the dynamic of thin films using holes opening experiments.[11] Russell et al. used fluorescence recovery after photobleaching to measure the chain diffusion in polystyrene thin film and found a reduction of the diffusion coefficient with decreasing film thickness.[13] They concluded that chain adsorption on the substrate is what reduces the chain diffusion. MacKenna et al. carried out mechanical tests using the "bubble inflation" technique on ultrathin films and suggested a strong reduction of rubbery compliance as the film thickness decreases.[14] Their results might infer that thin films exhibit a higher entanglement density than bulk. Bodiguel et al. conducted experiments on contractions induced by surface tension of ultrathin films.[15] They did not find any dependence of the rubbery plateau on film thickness. However, they proposed that the thin film viscosity increases with decreasing film thickness. Si et al. performed stretching experiments on freestanding films and proposed that intrachain entanglement decreases with decreasing film thickness.[16] Recently, Forrest et al. investigated the dynamics of the free surface layer of polystyrene films by looking at the time dependence of hole closure.[17] They suggest that the relaxation of the free surface exhibits a bulk behavior for temperatures close to bulk T_g and then strongly deviates from the bulk relaxation for temperatures below T_g.

Although polymers are often found nanoconfined in geometries such as spheres, little effort has been dedicated to the study of their glass transition[19−21] and dynamics. This information could be useful in many industrial and environmental applications; blends, copolymers, nanocomposites, colloids, coatings etc. One example is zero-volatile organic compounds (VOC) coating, which uses polymer nanoparticles in the film-making process.[22−24] VOCs are used in coatings to lower the particle T_g, which permits the fabrication of crack-free films at room temperature. If the T_g is reduced by decreasing the nanoparticle size, the use of VOCs could be avoided, which would have a positive impact on the environment. Another example is in nanoblends, where hard polymer nanoparticles are used to reinforce soft matrices. Reducing nanoparticle size would be counterproductive in this application if it causes the reduction of their T_g.[21]

* Corresponding author. E-mail: rharbi@ujf-grenoble.fr.
[†] Laboratoire de Rheologie, UJF/INPG/CNRS.
[‡] Institut Laué-Langevin.
[§] Laboratoire Léon Brillouin.

10.1021/ma802734j CCC: $40.75

The ability to study thin film geometry is hindered by possible artifacts due to the chain conformation and to the residual stress induced by spin coating. This problem has recently been raised by numerous reports[1,12] including Reiter et al.,[12] who showed that residual stress causes dewetting of thin film. It is therefore of utmost importance to study the properties of nanoconfined polymers in spherical geometries. Furthermore, there is also a need to develop new experiments to study the dynamics and nanomechanical properties of nanoconfined polymers in the nanoparticle geometry.

In this work we present a novel method that could be used to study the dynamics and nanomechanical properties of confined polymers in nanoparticles. Nanoblends of dPS/PBMA were prepared from a mixture of colloidal suspensions of cross-linked PBMA and a few percent of dPS nanoparticles via water evaporation. The polymer blends were prepared at temperatures well below the glass transition of PS (T_g^{PS}) and above the T_g of cross-linked PBMA particles (T_g^{PBMA}). In these conditions we expect the glassy PS nanoparticles to remain spherical and the cross-linked PBMA particles to deform under capillary pressure to fill the interstices between them, thus storing elastic energy. Upon annealing the films above T_g^{PS}, the PBMA nanoparticles regain their spherical shape and release the stored elastic energy, which then induces the deformation of the PS nanoparticles. Small angle neutron scattering was then used to monitor the shape evolution of the PS nanoparticles and to quantify the relaxation dynamics of the polystyrene nanoparticles.

2. Experimental Section

2.1. Materials. Monomers, deuterated styrene (D_8, Aldrich, 99%), nondeuterated styrene (Aldrich, 99%), butyl methacrylate (Aldrich, 99%) and cross-linker, ethylene glycol dimethylacrylate (EGDMA) were used as received. The surfactant, sodium dodecyl sulfate (SDS, Aldrich, 99%), the initiator, potassium persulfate (KPS, Aldrich, 98%), and buffer sodium bicarbonate were used as received. Double deionized water was used in the emulsion polymerization.

2.2. Synthesis. Polybutylmethacrylate (PBMA) and deuterated polystyrene (dPS) particles were prepared using emulsion polymerization at 80 °C. The polymer concentrations in water were 10 wt % for the PBMA and 2 wt % for dPS. The PBMA particles were cross-linked at 1, 10, and 20 wt % using ethylene glycol dimethylacrylate (EGDMA) during the polymerization. The PBMA nanoparticles were prepared in a standard 3 neck round flask (500 mL) with a condenser and a nitrogen inlet. The mixture (26 g) of cross-linker (EGDMA) and monomer (BMA) were added to the predegassed SDS (3 g)/water (250 g) solution, which was previously heated at 80 °C. The solution was vigorously agitated for 20 min before the initiator was added. A solution of the initiator KPS (33 mg) in water (1.7 g) was added to the reaction. After 4 h, another solution of the KPS (5.4 mg) in water (0.7 g) was added to polymerize all the non reacted monomer.

The polystyrene was either prepared from pure deuterated styrene D_8 or from a mixture 50/50 wt. % of deutertaed styrene D_8 and hydrogenated styrene. The dPS particles were prepared in a 50 mL minireactor equipped with a gas inlet and a homemade mini-condenser. The size of the dPS particles was controlled by varying the added amount of surfactant in the reaction. The mixture of water (18 g) and SDS (30 mg) was heated to 80 °C, under nitrogen flux for 20 min and then 0.3 g of styrene monomer (50/50 wt % deuterated and hydrogenated) was added. A solution of the initiator KPS (14 mg) in water (0.5 g) was added to the reaction. After 4 h, another solution of the KPS (1.4 mg) in water (0.25 g) was added to polymerize all the non reacted styrene monomer.

The surfactant and free ions were removed from the dispersions using a mixture of anionic and cationic exchange resins (Dowex, Aldrich). The suspensions were cleaned a few minutes prior to film preparation.

2.3. Polymer and Particle Characterization. The molecular weight was measured using gas permeation chromatography (GPC) in tetrahydrofuran (THF). The polystyrene was found to have a $M_w = 371 \times 10^3$ Da, $M_n = 216 \times 10^3$ Da and polymolecularity index PDI = 1.72 for the first sample (PS-YD5) and 280×10^3 Da, $M_n = 107.9 \times 10^3$ Da and PDI = 2.59 for the second (PS-YD3).

Table 1. Properties of the Samples Used

	PBMA-1	PBMA-10	PBMA-20	PS-YD5	PS-YD3
cross-linking, %	1	10	20	0	0
particle diameter, nm	50	55	60	80	83
size polydispersity index				0.042	0.037
T_g (°C)	36	55	broad	103	102

Particle diameter (D) was measured using Quasi Elastic Light Scattering (QELS) (Malvern 5000) at a 90° angle. CONTIN software was used for the QELS analysis. The particle diameter and size polydispersity are listed in Table 1. To make sure that the solution were not aggregated in water, the experiment were repeated at various angles from 70 to 130° and no angular dependence of the diameter was observed.

Differential scanning calorimetry (DSC) was carried out on a Mettler-Toledo DSC822 apparatus with a rate of 10 K/min for polystyrene and 40 K/min for highly cross-linked PBMA. Table 1 shows the properties of the particles and the polymers. High cross-linking PBMA particles 20% yield broad DSC curves, which makes it difficult taking a single T_g value. The experiments were carried out using PS-YD5, with some exceptions which were performed using PS-YD3; these were specified in the figure captions.

2.4. Rheometry Characterization of the Polymers. Shear modulus (G') measurements were carried out on AR-G2 (TA Instrument) for various frequencies and temperatures in a parallel plate geometry. With these measurements, the storage shear modulus G' and loss shear modulus G'' were calculated. All measurements were carried out in the linear viscoelastic regime in such a way that G' and G'' were independent of the applied stress. For cross-linked PBMA, the frequency ranged from 0.001 to 300 rad/s and the temperature from 20 to 140 °C. PBMA samples for rheometry were prepared using PBMA powder, predried at room temperature. The PBMA powder was pressed and heated at 120 °C to yield 1 mm thick films. Slightly tough, crack-free films were obtained for PBMA cross-linked up to 12.5%, whereas extremely fragile and cracked film was obtained in the PBMA cross-linked at 15 and 20 wt %. A thin layer (10 μm) of Lactite Superglue-3 (cyanoacrylate) was used to improve adhesion of the films onto the tools. The time−temperature shift factor (a_T) from the William−Landau−Ferry (WLF) equation was calculated using bulk T_g as the reference temperature. The rubbery G' values for PBMA were calculated at a frequency of 1 rad/s for temperatures between 95 and 140 °C.

2.5. Preparation of Blends for Neutron Scattering Experiments. The surfactant and free ions were removed from the dispersions using a mixture of anionic and cationic exchange resins (Dowex, Aldrich). The polystyrene suspensions were annealed in a stainless steel bomb at 120 °C for 20 min in order to release the thermal history. The nanoblends were prepared by mixing dPS and PBMA dispersions to make dPS concentrations of 2 wt % of the solid PBMA. Cracked films were obtained after water evaporation at 56 °C.

2.6. Small Angle Neutron Scattering Experiments. The small angle neutron scattering (SANS) experiments were carried out on spectrometer PAXY of Laboratoire Léon Brillouin (LLB, Saclay) at the reactor Orphée Saclay and at D22 and D11 of Institut Laué-Langevin (ILL, Grenoble). The scattered neutrons were collected on an XY bidimensional multidetector, and the counts were regrouped according to circular rings to yield spectra of intensities $I(q)$ versus the magnitude of the scattering vector modulus (q). The range of accessible q values was between 0.0022 and 0.1 Å^{-1}. The samples were prepared by gently grinding the cracked film into a powder with grains of 0.5 mm beads. 105 mg of this powder was then introduced between two quartz disks separated by a spacer of 12 mm inner diameter and 1.2 mm thickness. In one set of

Scheme 1. Description of the Experimental Procedure

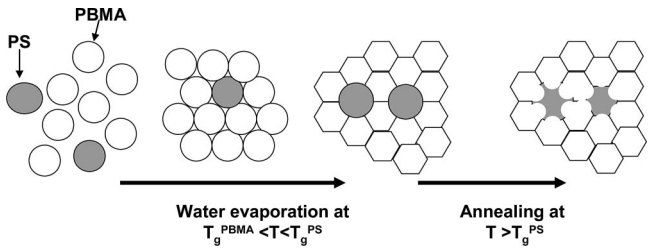

experiments, sample annealing was carried out ex situ in an oven at a controlled temperature. In these experiments, the samples were annealed, quenched to room temperature, measured and then annealed again. This cycle was repeated several times. In the second type of experiment (in situ), the sample was positioned in the neutron beam in a home-built oven equipped with two quartz windows and was heated to the desired temperature during the SANS measurements. The sample temperatures were monitored using a thin thermocouple placed in proximity of the sample. The sample temperature was found to reach the desired temperature within 2 min. One minute neutron spectra were taken at various annealing times.

The evolution of the SANS spectra with time was monitored either by following the variation of the scattering intensity at various q values $I(q)$ or by monitoring the evolution of the gyration radius (R_g) with the annealing time. The R_g is calculated by fitting the low q values of $I(q)$ using the Guinier representation, $\ln(I(q) = \ln(I(0)) - q^2 \times R_g^2/3$.

3. Results and Discussion

3.1. Protocol for Measuring Nanomechanical Properties of Polystyrene Nanoparticles. The short scale dynamic of polymer thin film has mainly been investigated using the dielectric relaxation technique.[4] Whereas, the large-scale dynamic of nanoconfined polymers have been studied by various methods including 1) film dewetting,[12] film contraction[15] and nanobubble inflation used to measure the dynamics of thin films,[14] 2) nanoparticle imbedding and healing of deformed surfaces used to monitor the dynamics of polymer free surfaces,[17] and 3) polymer diffusion in cylindrical pores.[18] In this paper we present a new protocol for monitoring the relaxation of polystyrene nanoconfined in nanoparticles. Nanoblends of dPS/PBMA were prepared from a mixture of colloidal suspensions of cross-linked PBMA and a small fraction of dPS nanoparticles (1−2%) via water evaporation, see Scheme 1. The polymer blends were prepared at temperatures well below the glass transition of PS (T_g^{PS}) and above the T_g of cross-linked PBMA particles (T_g^{PBMA}). In these conditions we expect the PBMA particles to deform under capillary pressure to fill the interstices between them and the glassy PS nanoparticles to remain spherical. The applied capillary pressure during the closure of the interstices $G = 12.9\gamma_{aw}/R$, (where γ_{aw} is the surface tension of air/water and R is the radius of the particle) is in the order of G $\sim$ 23 MPa for the particles investigated here. Thus, the glassy PS particles (G $\sim$ GPa) are expected to remain spherical at the temperature of film formation (T^f). Whereas the cross-linked PBMA particles, which exhibit an elastic modulus of G < 23 MPa should deform under Laplace pressure for $T^f > T_g^{PBMA}$, and therefore elastic energy is stored within the PBMA nanoparticles. Upon annealing the nanoblends above T_g^{PS}, the PBMA nanoparticles surrounding the PS particles release the stored elastic energy by partially regaining their spherical shape, which induces the deformation of the PS nanoparticles as proposed in Scheme 1. SANS is then used to monitor the shape evolution of the PS nanoparticle and to quantify the relaxation dynamic of the polystyrene nanoparticles.

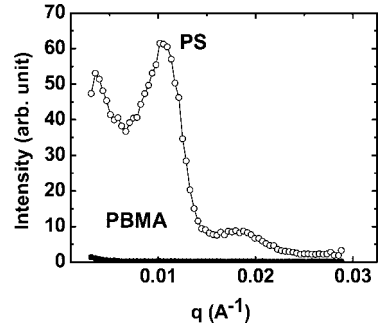

Figure 1. SANS spectra of film made from a suspension of 10% cross-linked PBMA particles (56 nm) (●) compared to SANS spectra of film made from a suspension of polystyrene nanoparticles (62 nm) (○). The films were prepared by evaporation at 56 °C.

3.2. Structure of dPS and PBMA Nanoparticles before Annealing. In Figure 1, we show the SANS spectra of films made by evaporation at 56 °C of cross-linked PBMA nanoparticles of diameter 56 nm (filled symbol), compared with SANS spectra of films also made at 56 °C from suspensions of glassy polystyrene nanoparticles (62 nm diameter) (open symbol). The films made from suspensions of glassy polystyrene nanoparticles at a temperature (56 °C) well below their bulk T_g (100 °C) yield strong scattering peaks (Figure 1). The scattering peaks show that the glassy dPS particles remain almost spherical and separated by the interstices. Because the glassy elastic modulus of these particles is in the order of GPa, the Laplace pressure is insufficient to deform the nanoparticle and to close the interstices. Since the particles have a monodisperse size distribution, the evaporation results in a packing of the particles into a long-range ordered cubic face centered (CFC) structure, which would yield scattering peaks with the first peak at $q = 2\pi/D_{PBMA} = 0.01$ Å^{-1}.

On the contrary, the SANS of the PBMA nanoparticles (filled circles) is very weak and shows no structure for any $q > 4\times 10^{-3}$ Å^{-1}. This suggests that films formed via evaporation of cross-linked PBMA suspensions above their glass transition are uniform at the microscopic scale and that the cross-linked PBMA nanoparticles deform under Laplace pressure to fill the void (interstices) between them. If the PBMA particles were to remain spherical after water evaporation, the contrast between the particles and interstices would result in a noticeable scattering peak at $q = 2\pi/D_{PBMA} = 0.01$ Å^{-1}.

In Figure 2, we show the SANS spectra of blend films containing 2 wt % dPS dispersed in a 10% cross-linked PBMA matrix. The spectra exhibit a continuously decreasing scattering intensity $I(q)$, which can safely be attributed to the 2% deuterated dPS particles in the cross-linked PBMA matrix. In principle, $I(q)$ is the product of the form factor $P(q)$ and the structure factor $S(q)$ of the dPS particles $I(q) = P(q)\times S(q)$. The structure factor $S(q) = 1$ because of a low dPS concentration and the absence of selective aggregation, which yields $I(q) = P(q)$. The $I(q)$ intensities were compared to the $P(q)$ of polydispersed hard spheres and the diameter and polydispersity of the particles were calculated from the best fit (Figure 2). These diameters are similar to those from quasi elastic light scattering. The best fit was found for particle diameter 78 nm and polydispersity index PDI = 5%. This infers that the dPS nanoparticles are indubitably individually dispersed within the PBMA matrices and remain spherical in the blends. Moreover, these spectra indicate that here, like in Figure 1, the PBMA particles are deformed under Laplace pressure to fill the interstices. Otherwise, a strong scattering peak from the PBMA matrix at $q = 2\pi/D_{PBMA} = 0.01$ Å^{-1} would be visible.

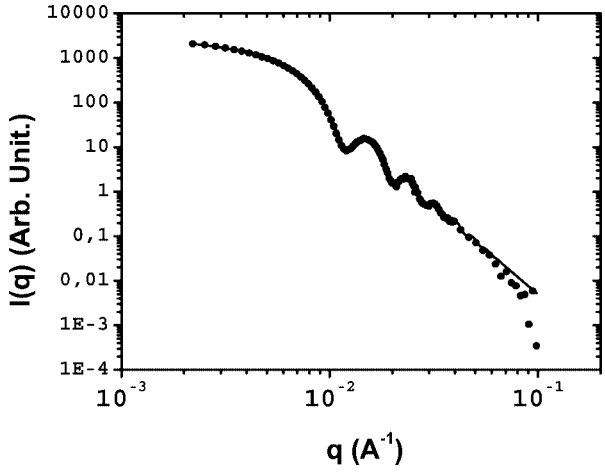

Figure 2. SANS spectra of film made from 2 wt % deuterated polystyrene particles (80 nm) dispersed in a 10% cross-linked PBMA matrix. The films were prepared from a mixture of two suspensions; 10% cross-linked PBMA particles (56 nm) and 80 nm dPS nanoparticles. The films were prepared by evaporation at 56 °C (above T_g of PBMA and below T_g of dPS). The SANS curve is fitted to a form factor of polydispersed spheres with a diameter of 78 nm and a polydispersity PDI = 5%.

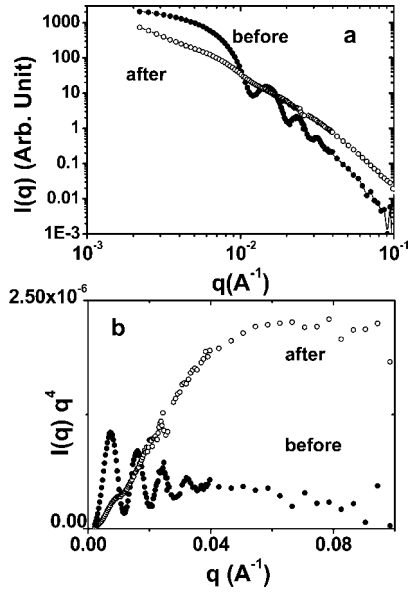

Figure 3. SANS spectra of 80 nm polystyrene nanoparticles (2 wt %) in a 10% cross-linked PBMA matrix before annealing (●) and after annealing at 140 °C for 1 h (○). (a) Plot of the scattering intensity $I(q)$ vs q and (b) plot of $q^4 \times I(q)$ vs q.

3.3. Structure of the dPS Nanoparticles after Annealing. Figure 3 shows that when the films made from 2% dPS nanoparticles in a 10% cross-linked PBMA matrix are annealed at 140 °C, the oscillations of the scattering spectra progressively disappear, the scattering intensity $I(q)$ decreases for $q < 0.01$ Å^{-1} and increases for $q > 0.01$ Å^{-1}. The evolution of the SANS spectra shows that the shape of the dPS nanoparticles, or their spatial distribution, evolve during the annealing process. Such change could either result from (1) fusion of several particles, which were in contact prior to annealing, (2) dissolution of deuterated low molecular weight polystyrene chains into the PBMA matrix, or (3) deformation of the individual dPS particles.

One could imagine that the change in the SANS spectra results from penetration of deuterated polystyrene chains in the PBMA matrix. Polystyrene and uncrosslinked PBMA form an

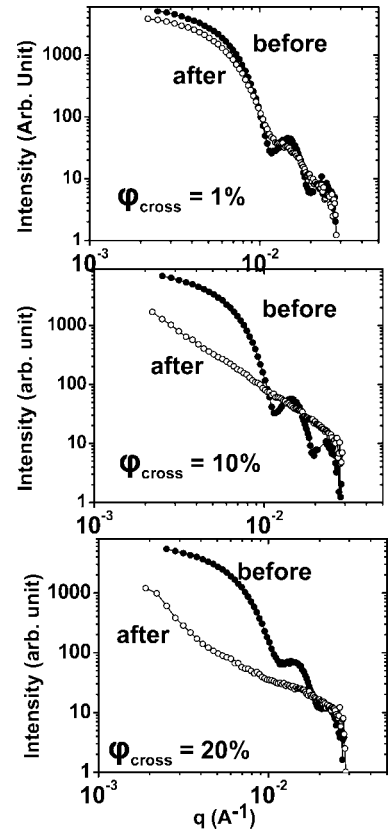

Figure 4. SANS spectra of 83 nm polystyrene nanoparticles (2 wt %) in a cross-linked PBMA matrix before annealing (●) and after annealing at 140 °C for 1 h (○). The PBMA matrix was cross-linked to 1%, 5%, 10%, and 20%. The polystyrene particles used here are PS-YD3.

interface which is a few nanometers thick,[25] whereas highly cross-linked PBMA is likely to inhibit the interpenetration of the polymers. If fusion of dPS nanoparticles or penetration of dPS into the PBMA matrix is what causes the observed transformation in the SANS spectra, then the change should be more enhanced in low cross-linked PBMA matrices. In contrast with this, the spectra of films made of low cross-linked PBMA matrices remain slightly the same upon annealing and when the cross-linking ratio (φ_{cross}) was varied from 1 to 20%, the highest φ_{cross} was found to yield the highest magnitude of change in the SANS spectra (Figure 4). Therefore the possibility that fusion dPS particles or penetration of dPS in the PBMA matrix is what causes the observed change in $I(q)$ can be safely discarded.

Fusion can be also discarded for other reasons. First, a very direct and strong one is that since it would yield large particles, the total surface area of the particles would be lower. This specific interface area between the dPS and the PBMA can be calculated from the value of $q^4 \times I(q)$ at large q, following the Porod law. We see in Figure 3b that the average value of $q^4 \times I(q)$ triples after annealing at 140 °C, whereas fusion between particles is expected to lead to a reduction of the total surface area.

Second, fusion should yield large particles and a high scattering intensity for $q \rightarrow 0$ ($I(0) \sim \varphi V_{part}$, where φ is the volume fraction and V_{part} is the volume of the particles). The measured $I(q)$ for low q values in the annealed films were always found to be lower than the $I(q)$ of the nonannealed films in the range of q values investigated. This infers that the shape of dPS particles changes during annealing while their volume remains the same. To confirm this, simulation of the form factor of aggregated particles was performed, where the pair correlation function ($g(r)$) of aggregates made of a few particles was

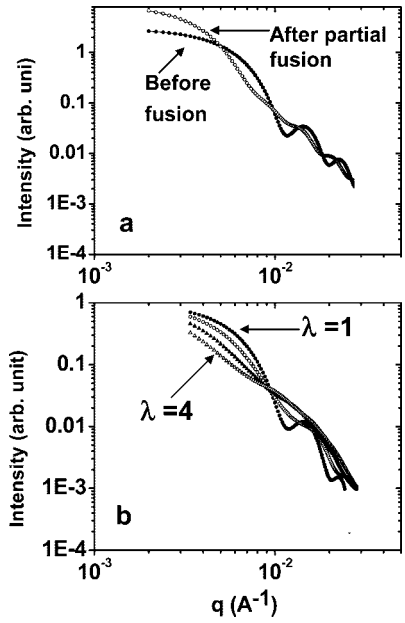

Figure 5. (a) Simulated scattering spectra from an aggregate made of 3 spherical particles (80 nm) before their fusion (●) and after their partial fusion (○). (b) Simulated scattering spectra of 80 nm particles deformed into a star-like shape with 12 branches. The star-like shape is formed by connecting 6 prolate ellipsoids in a CFC geometry. The ellipsoid is characterized by a factor λ = length/ width and its size is calculated in such a way as to yield a star-like particle of the same volume as the 80 nm particle. (●) spectra of the nondeformed particle $\lambda = 1$, (○) $\lambda = 2$, (▲) $\lambda = 3$ and (△) $\lambda = 4$.

calculated and used in the computation of the scattering intensity $I(q) = \int g(r) \sin(qr)/(qr)\, dr$.[26] In Figure 5, we plot an example of simulated spectra of three nanoparticles in contact, at various steps of their fusion. As the particles fuse together their total volume increases and the calculated $I(q)$ at low q values increases above the $I(q)$ of the individual particles.

It is therefore clear that fusion of dPS nanoparticles and penetration of dPS into the PBMA matrix are not responsible for the observed transformation of the SANS spectra upon annealing. The change of SANS spectra most likely results from the deformation of individual polystyrene nanoparticles in the cross-linked PBMA matrix.

3.4. Shape of the Particles after Annealing. After annealing of the PS/PBMA nanoblends the dPS nanoparticles undergo a deformation which is dictated by the behavior of the surrounding cross-linked PBMA particles. To explain how the dPS nanoparticles deform we propose the following mechanism: during annealing, the cross-linked PBMA particles regain their spherical shape and squeeze the dPS particles between them. This mechanism is likely to produce a dPS nanoparticle with an elongated shape with many branches extending from it. The simplest picture is that the dPS nanoparticles deform into a star-like shape with 12 branches according to Scheme 1.

The star-like particle with 12 branches was simulated by connecting 6 prolate ellipsoids positioned in the face centered cubic geometry (CFC). The prolate ellipsoids have an aspect factor λ = length/width and their dimensions were calculated in such a way as to yield a star-like particle of the same volume as the 80 nm particle. The pair correlation function ($g(r)$) of these particles was calculated and used in the computation of the scattering intensity $I(q) = \int g(r) \sin(qr)/(qr)\, dr$.[26] In Figure 5b, we show the evolution of the calculated scattering intensity as the particles deform from the spherical shape to the elongated star-like shape. For low q values, the scattering intensity of the star-like particle is lower than the $I(q)$ of the spherical particles: this is because the larger radius of gyration implies a faster decrease of $I(q)$ with q (the limit at $qR_g < 1$ does not change since the volume stays the same, but it has moved out of our available q range). For high q values, the calculated $I(q)$ of the star-like shape is higher than that of the sphere as expected from the Porod law since the specific area is larger. The shape of the simulated spectra of the star-like particles of Figure 5b qualitatively resembles the SANS spectra of the annealed film of Figure 3. It is therefore strongly probable that the dPS particles deform into an elongated form with many branches in a similar manner as described in Scheme 1.

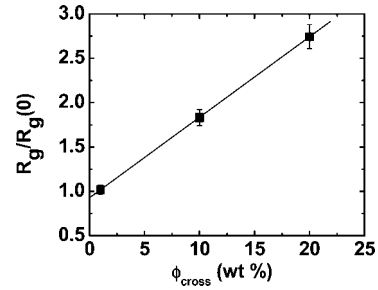

Figure 6. The ratio of the gyration radius of dPS particles ($R_g/R_g(0)$) before and after annealing the films at 140 °C, plotted against the cross-linking ratio. The R_g is calculated by fitting the low q value of $I(q)$ from Figure 4 to the Guinier plot. The polystyrene particles used here are PS-YD3.

3.5. Attempt to Estimate the Relaxation Shear Stress of the Polystyrene Nanoparticle. In Figure 4, we show that a low cross-linked PBMA matrix (1%) yields a small change in the shape of the PS particles, whereas 10% and 20% cross-linked matrices lead to increasingly significant changes in the shape the PS particles. We quantify the rate of deformation of the dPS nanoparticles by using the ratio of the gyration radius before ($R_g(0)$) and after annealing $R_g/R_g(0)$ (Figure S1 of the Supporting Information). In Figure 6, we plot the maximum rate of deformation, $\lambda^{max} = R_g/R_g(0)$, of films annealed for 40 min at 140 °C versus the cross-linking ratio (φ_{cross}) of the PBMA matrices. The $\lambda^{max} = R_g/R_g(0)$ increases linearly with φ_{cross} for all the samples investigated. The Laplace pressure P_{lap} between the PS and PBMA ($P_{lap} \propto \gamma_{PS\text{-}PBMA}A$) tends to minimize the total surface area of contact between the polymers (A) and therefore acts as a barrier against the deviation of PS particles from the spherical shape. In uncrosslinked PBMA, the Laplace pressure is sufficient to inhibit the deformation of PS particles. Beyond 1% cross-linking ratio, the elastic stress stored in the PBMA particles can overcome the Laplace pressure (P_{lap}) and the magnitude of deformation increases linearly with increasing φ_{cross} (Figure 6). The Laplace pressure of the spherical particle $P_{lap} = 4\gamma_{PS\text{-}PBMA}/D_{PS}$, where $\gamma_{PS\text{-}PBMA}$ is the surface tension between PS and PBMA and D_{PS} is the diameter of the PS particle. By using $\gamma_{PS\text{-}PBMA} = 0.72$ mN/m[27] we can estimate the Laplace pressure to be $P_{lap} = 0.036$ MPa, which is four times lower than the bulk shear modulus of the 1% cross-linked matrix G' (140 °C) = 0.15 MPa. In all our experimental conditions the Laplace pressure is well below the elastic modulus of the cross-linked PBMA matrix and therefore it should not play a significant role in counterbalancing the applied stress. The bulk elastic shear modulus measured at 140 °C is found to increase linearly with the φ_{cross} (0.15 MPa, 4.7 MPa and about 10 MPa for 1%, 10% and 20% respectively). Therefore the deformation rate as defined by $\lambda^{max} = R_g/R_g(0)$ is found to increase linearly with increasing elastic shear modulus of the surrounding matrix as $\lambda^{max} = R_g/R_g(0) = 1 + 0.22\times G'$.

The deformation of the polystyrene particle could be schematized as depicted in Scheme 2. The cross-linked PBMA particles in the aqueous phase are spherical and deform under capillary pressure around the PS particles during film formation

Scheme 2. Zoomed View of the Deformation of Polystyrene Particles[a]

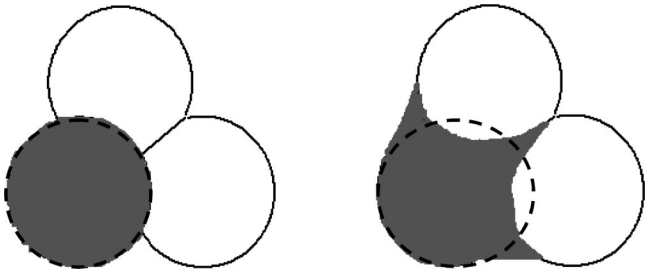

[a] The dark particles represent PS and the white particles are the cross-linked PBMA particles: (left) before annealing and (right) after annealing. The dashed circle represents the position of the PS particle before deformation.

to fill the voids left by the evaporation of water. The stored elastic stress in the PBMA particles should be proportional to the elastic modulus of the PBMA and the extent of deviation of the PBMA particles from the spherical shape. Upon annealing, the stored elastic stress is released when the PS particles deform into an elongated shape and the PBMA regain their spherical shape to some extent. The relationship between strain and stress in this system can be written as

$$\int_0^t G_{PS}(t-t')\frac{d\varepsilon_{PS}}{dt'}\,dt' = -\int_0^t G_{PBMA}(t-t')\frac{d\varepsilon_{PBMA}}{dt'}\,dt' \quad (1)$$

$$\int_0^t G_{PS}(t-t')\frac{d\varepsilon_{PS}}{dt'}\,dt' = G_{PBMA}(\varepsilon_{PBMA}(0) - \varepsilon_{PBMA}(t)) \quad (2)$$

where $G_{PS}(t)$, G_{PBMA} are the relaxation shear modulus of the PS and the PBMA particles and ε_{PS}, ε_{PBMA} are the deformation strain of the PS and the PBMA particles. Within the time of the experiment, the $G_{PBMA}(t)$ contains only the elastic component of the shear modulus at temperatures higher than the T_g of PBMA and therefore G_{PBMA} could be considered constant (eq 2). If one assumes that the strains of the PS (ε_{PS}) and PBMA (ε_{PBMA}) exhibit an exponential behavior with a relaxation time (τ), the relaxation modulus $G_{PS}(t)$ should also vary exponentially with the same characteristic time τ. However, because the PS particles undergo deformation in three dimensions, at this stage we do not attempt to derive the absolute value of the relaxation shear modulus of the nanoconfined polystyrene based on these experiments. Nevertheless, we derive the relaxation time of the shear modulus which could be used to gain insight on the relaxation dynamic of nanoconfined polystyrene in nanoblends.

3.6. Dynamics of Deformation of Polystyrene Nanoconfined in Nanoblends at Temperatures above the Bulk Glass Transition. In Figure 7 we show the SANS spectra I(q) at various annealing times for 80 nm polystyrene nanoparticles in a 10% cross-linked PBMA matrix, annealed at 140 °C. The change in the SANS spectra takes over 30 min at 140 °C. In order to quantify the dynamics of the polystyrene nanoparticles using the change in the spectra of Figure 7, we can either exploit (1) the variation with time of the gyration radius R_g of the PS particle, calculated from the Guinier plot or (2) the change of the scattering intensity at various q values.

In Figure 8a, we show the plot of $(R_g(t)/R_g(0))$ against the annealing time, where $R_g(t)$ is the gyration radius at various annealing times and $R_g(0)$ is the gyration radius before annealing. The $R_g(t)/R_g(0)$ decay fits perfectly to a stretched exponential with a decay time of $\tau_{Rg} = 11$ min and $\beta = 0.72$. When the decay was compared to a single exponential expression, the fit was fairly acceptable with $\tau_{Rg} = 8.2$ min.

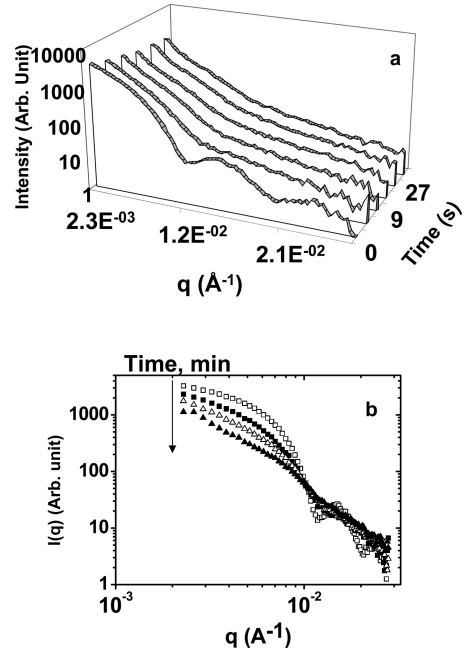

Figure 7. (a) 3D representation of the evolution of the scattering spectra ($I(q)$ vs q) plotted for various annealing times for 80 nm dPS nanoparticles in a 10% cross-linked PBMA matrix. (b) 2D representation of the evolution of the scattering intensity at different annealing times: (□) before annealing; after (■) 4 min, (△) 17 min, and (▲) 37 min. The films were annealed at 140 °C.

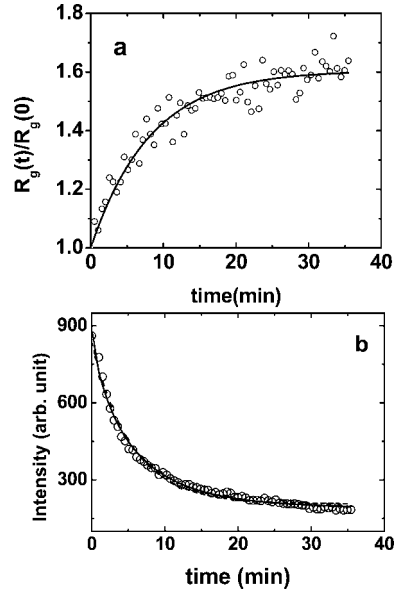

Figure 8. (a) $R_g(t)/R_g(0)$ vs the annealing time for film made from 80 nm dPS nanoparticles in 10% cross-linked PBMA annealed at 140 °C. R_g is calculated using the Guinier representation. The curve fits to a single exponential with $\tau = 4.2$ min (continuous line). (b) Evolution of the scattering intensity at $q = 0.00504$ Å^{-1} as a function of the annealing time. The plot is fitted to a single exponential (continuous line) with a $\tau = 4.54$ min and to a stretched exponential (dashed line) with $\tau = 4.89$ min and $\beta = 0.716$.

In Figure 8b, we show the evolution of $I(q)$ with time for films annealed at 140 °C for the particular case of $q = 0.00504$ Å^{-1}. This plot also fits perfectly to a stretched exponential with $\tau = 4.89$ min and an exponent of $\beta = 0.716$ (Figure S2, Supporting Information). It also fairly fits to a single exponential expression with $\tau = 4.54$ min, which is close to that found from the fit to the stretched exponential (Figure 8b). However this decay does not fit the stretched exponential for $\beta = 0.4$, in

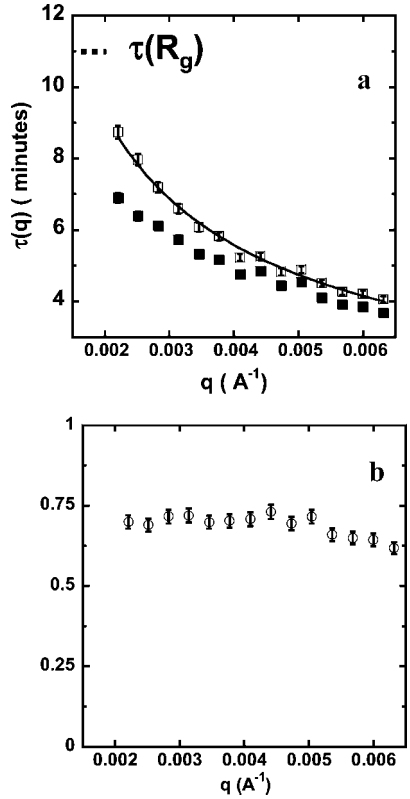

Figure 9. (a) Relaxation time $\tau(q)$ plotted against q. $\tau(q)$ is calculated from the fit of the scattering intensities ($I(q)$ vs time) of Figure 8 to a single exponential (■) and to a stretched exponential (□). The dashed line is the τ calculated from the fit of $R_g(t)/R_g(0)$ vs time of Figure 8 to a single exponential. (b) Exponent β, calculated from the fit of scattering intensities vs time of Figure 8 to a stretched exponential, plotted against q.

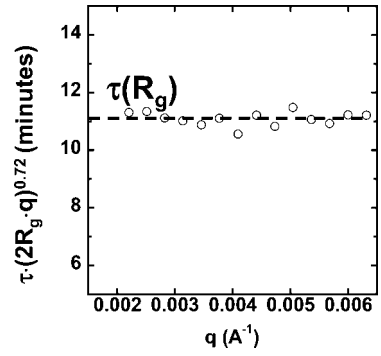

Figure 10. Normalized relaxation time $\tau^* = \tau(q/q^*)^{0.72}$, plotted against q, where q^* is chosen as $q^* = 1/(2R_g)$. τ is calculated by fitting the scattering intensity vs time to a single exponential. The dashed line is the $\tau(R_g)$ calculated from the fit of $R_g(t)/R_g(0)$ vs time of Figure 8 to a single exponential.

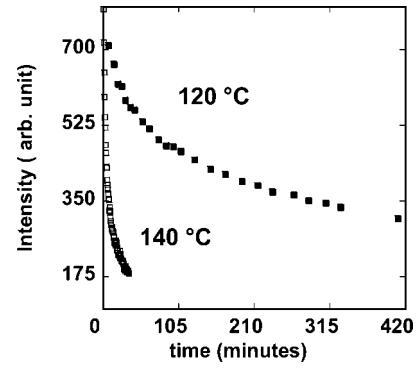

Figure 11. Evolution of the scattering intensity at $q = 0.00504$ Å^{-1} as a function of the annealing time at 140 °C (□) and 120 °C (■).

contrast to the relaxation function of bulk polystyrene (Figure S2 of the Supporting Information). Although the decays are clearly stretched exponentials with an exponent $\beta = 0.716$, we will nonetheless also use the results of the fit to a single exponential to provide a rough estimation of the average characteristic time. The least-squares (χ) was calculated for various β values and plotted in the Figure S3 of the Supporting Information. The width of the minimum of the least-squares gives an idea on the reliability of the fit and an estimation of the error bar in β and τ. Because the width at the minimum of χ is quite narrow we can conclude that β and the corresponding τ can be estimated with a precision of less than 3% at 140 °C. For $q = 0.00504$ Å^{-1} β was found to be $\beta = 0.716 \pm 3\%$ and $\tau = 4.89 \pm 1\%$. Since the stretched exponential dynamics are dominated by the longer relaxation times, we should calculate the average relaxation times $\langle\tau\rangle$.[29] $\langle\tau\rangle$ was calculated as $\langle\tau\rangle = \int \exp(-(t/\tau)^\beta)\, dt$ using τ and β values from the fit to the stretched exponential and was found to be $\langle\tau\rangle = 5.089 \pm 3.3\%$ for $q = 0.00504$ Å^{-1}.

The fits of the decays to the stretched exponential and single exponential for different q values yielded τ(q) values which decrease with increasing q from 8.7 to 4.04 min for q values between 2.5×10^{-3} Å^{-1} and 6.5×10^{-3} Å^{-1} (Figure 9a). The exponent β is found to be constant at $\beta = 0.708 \pm 0.025$ for $q < 0.00504$ Å^{-1}, which is also equal to the β value found from the fit of the gyration radius. For $q > 0.00504$ Å^{-1} β was found to decrease with increasing q and for $q = 0.0065$ Å^{-1} $\beta = 0.625$ (Figure 9b).

Since $I(q)$ at each q value portrays the density fluctuations with a size of $\xi = 2\pi/q$, $\tau(q)$ also describes the relaxation dynamic of the density fluctuation with a size of ξ. Larger fluctuations would require more time to change than a smaller fluctuation. Therefore $\tau(q)$ increases with increasing ξ and thus increases with deceasing q. For q approaching $q = 0$, $\tau(q)$ converges toward the relaxation time of the gyration radius τ_{Rg}, which is the largest size of the system. The $\tau(q)$ was found to follow a power law behavior (τ(q) $\propto q^{-\alpha}$) with an exponent $\alpha = 0.72$ in the range of $q < 0.0065$ Å^{-1}. Whereas the characteristic time calculated from the dynamic of the structure factor ($\tau(q)$) of a Gaussian polymer chain is expected to vary as $\tau(q) = Dq^2$, in the low q range.[28] Simulations of the deformation of the particles from sphere to star like shape were performed by imposing the gyration radius to increase as a stretched exponential with $\tau = 11$ min and $\beta = 0.72$ and the $\tau(q)$ was calculated for various q values. The simulation yielded a decrease in $\tau(q)$ with increasing q as $\tau(q) \propto q^{-\alpha}$ with $\alpha = 1.16$.

The dynamics of polystyrene nanoparticles could be characterized either by using the relaxation time of the gyration radius (τ_{Rg}) or by using a normalized τ(q), $\tau^* = \tau(q) \times (q/q^*)^{0.72}$, where τ^* is an apparent characteristic time independent of q and q^* is constant (Figure 10. We chose $q^* = 1/(2R_g)$, which corresponds to $\xi = 2R_g$. At 140 °C, τ^* is found to be constant for the low q range $q < 0.0065$ Å^{-1} and equal to τ_{R_g} ($\tau^* = \tau_{R_g} = 11$ min).

In Figure 11, we compare the decay of the scattering intensity $I(q)$ vs time at 140 and 120 °C for $q = 0.00504$ Å^{-1}. The fit to a stretched exponential gives a relaxation time $\tau(q)$ which increases from 4.89 min ± 1% at 140 °C to 130.5 min ± 1% at 120 °C and an exponent β, which decreases from 0.716 at 140 °C to 0.44 at 120 °C for $q = 0.00504$ Å^{-1} (Figure S2 and S3 of the Supporting Information). At 120 °C, $\tau(q)$ was also found to decrease with increasing q in the same manner as in Figure 9a from 238 to 130.5 min for q between 0.0022 and 0.00504 Å^{-1}. In contrast with 140 °C, the β at 120 °C was found to decrease from 0.48 to 0.44 for q varying between 0.0022

and 0.00504 $Å^{-1}$ with a mean value of $\beta = 0.46 \pm 0.02$. Reference 29 also reported that β in bulk polystyrene decreases with decreasing temperature from 0.51 at 128 °C to 0.24 close to bulk T_g.

The shift factor a_T is calculated using the relaxation time from the two temperatures, and is compared to the Vogel−Fulcher−Tamman (VFT) model $\tau = \tau^0 \exp(B/(T - T_0))$, where T_0 is the temperature at which the relaxation time diverges and B the apparent activation energy. One could also use the VFT model to derive the Williams−Landel−Ferry (WLF) equation with $C_1 = B(T_g - T_0)$ and $C_2 = T_g - T_0$. For bulk polystyrene, C_1 is reported to range between 12.7 and 13.7, $C_2 = 49.9$ K, $T_0 = 323$ K, and $B = 1490$ K.[30] The a_T is calculated either using τ from the fit to a stretched exponential or otherwise $\langle\tau\rangle$. The a_T calculated using τ, is compatible with T_0 varying between 305.5 K and 307.2 K for q between 0.0022 $Å^{-1}$ and 0.00504 $Å^{-1}$ with an average value $T_0 = 306.7 \pm 1.2$ K if B is equal to the bulk value ($B = 1490$ K°). The calculated T_0 is 16.3 K ± 1.2K lower than T_0 for bulk polystyrene, which could suggest that the T_g of polystyrene nanoparticle is 16.3 K ± 1.2K lower than bulk T_g. If T_0 is taken as the bulk value ($T_0 = 323$ K), the comparison of a_T with VFT gives a $B = 957$ K°, which is smaller than the bulk value $B = 1490$ K°.

Since the stretched exponential dynamics are dominated by the longer relaxation times, we should calculate a_T using the average relaxation times $\langle\tau\rangle$.[29] The a_T calculated from $\langle\tau\rangle$ is compatible with T_0 ranging from 313.3 to 316.3 K for q varying between 0.0022 and 0.00504 $Å^{-1}$ if B is equal to the bulk value $B = 1490$ K°. This leads to an average value of $T_0 = 314.5$ K ± 1.8 K, which is 8.5 K ± 1.8 K lower than the T_0 of bulk polystyrene. This could infer that the T_g of the polystyrene nanoparticle is reduced by 8.5 K ± 1.8 K below bulk value. These results infer that the dynamic of polystyrene in the interfacial zone is affected by the dynamic of the surrounding PBMA matrix, which could induce either a reduction of the glass transition or the activation energy. These results show that this method can be used to gain a deeper insight into the dynamic of nanoconfined polystyrene in nanoblends; however, further experiments at various temperatures are necessary to fully describe the dynamic of nanoconfined polystyrene in nanoparticles.

4. Conclusion

We have developed a new method for measuring the nanomechanical properties and large scale dynamics of nanoconfined polymers in nanoparticles. Glassy polystyrene nanoparticles are dispersed in a highly elastic PBMA matrix made of cross-linked PBMA particles. The nanoblends are prepared at a temperature for which the elastic PBMA particles deform around the glassy spherical polystyrene particles. Upon annealing of the nanoblends, the elastic PBMA particles regain their spherical shape and the glassy PS nanoparticles deform under the affect of the elastic stress from the PBMA particles. The shape of the PS nanoparticles is monitored via SANS. The analysis of the SANS spectra infers that the shape of the polystyrene nanoparticle evolves from a spherical shape to a star-like shape with 12 branches. The time evolution of the particle shape is used to estimate the relaxation time (τ) of the nanoconfined polystyrene at 40 °C above bulk T_g. The dependence of the τ on the temperature and on the particle size will be used in further studies to extract some information on the large scale dynamics of nanoconfined polystyrene.

Acknowledgment. We thank Dr. Amine Ammar and Dr. Bechir Mokdad for stimulating discussions and Dr. H. Galliard for her help with these experiments. We thank the French Ministry of Education and the MACODEV program for their financial support.

Supporting Information Available: Figures showing a Guinier plot, the evolution of the scattering intensity as a function of the annealing time, and the least squares χ from fitting the decays of the scattering intensity. This material is available free of charge via the Internet at http://pubs.acs.org.

References and Notes

(1) Alcoutlabi, M.; McKenna, G. B. *J. Phys.: Condens. Matter* **2005**, *17*, 461.
(2) Forrest, J. A.; Dalnoki-Veress, K.; Stevens, J. R.; Dutcher, J. R. *Phys. Rev. Lett.* **1996**, *77*, 2002.
(3) Keddie, J. L.; Jones, R. A. L.; Cory, R. A. *Europhys. Lett.* **1994**, *27*, 59.
(4) Fukao, K.; Miyamoto, Y. *Phys. Rev. E.* **2000**, *61*, 1743.
(5) Kawana, S.; Jones, R. A. L. *Phys. Rev. E* **2001**, *63*, 021501.
(6) DeMaggio, G. B.; et al. *Phys. Rev. Lett.* **1997**, *78*, 1524.
(7) Ellison, C. J.; Torkelson, J. M. *Nat. Mater.* **2003**, *2*, 695.
(8) Varnik, F.; Baschnagel, J.; Binder, K. *Phys. Rev. E* **2002**, *65*, 021507.
(9) Riggleman, R. A.; Yoshimoto, K.; Douglas, J. F.; dePablo, J. J. *Phys. Rev. Lett.* **2006**, *97*, 045502.
(10) Forrest, J. A. *Eur. Phys. J. E* **2002**, *8*, 261.
(11) Roth, C. B.; Dutcher, J. R. *Phys. Rev. E,* **2005**, *72*, 021803.
(12) Reiter, G.; Hamieh, M.; Damman, P.; Sclavons, S.; Gabriele, S.; Vilmin, T.; Raphaël, E. *Nat. Mater.* **2005**, *4*, 754.
(13) Frank, B.; Gast, A. P.; Russel, T. P.; Brown, H. R.; Hawker, C. *Macromolecules* **1996**, *29*, 6531.
(14) O'Connell, P. A.; McKenna, G. B. *Science* **2005**, *307*, 1760.
(15) Bodiguel, H.; Fretigny, C. *Phys. Rev. Lett.* **2006**, *97*, 266105.
(16) Si, L. M; Massa, V.; Dalnoki-Veress, K.; Brown, H. R.; Jones, R. A. L *Phys. Rev. Lett.* **2005**, *78*, 127801.
(17) Fakhraai, Z.; Forrest, J. A. *Science* **2008**, *319*, 600.
(18) Shin, K.; Obukhov, S.; Chen, J.-T.; Huh, J.; Mok, S.; Dobryal, P.; Thiyagarajan, P.; Russell, T. P. *Nature Mats.* **2007**, *6*, 961.
(19) Sasaki, T., et al., *J. Chem. Phys.* **2003**, *119*, 8730.
(20) Herminghaus, S.; Seemann, R; Landfester, K. *Phys. Rev. Lett.* **2004**, *93*, 017801.
(21) Rharbi, Y. *Phys. Rev. E* **2008**, *77*, 031806.
(22) Winnik, M. A. Latex film formation. *Curr. Opin. Colloid Interface Sci.* **1997**, *2*, 192.
(23) Rharbi, Y.; Boué, F.; Joanicot, M.; Cabane, B. *Macromolecules* **1996**, *29*, 4346.
(24) Nawaz, Q.; Rharbi, Y. *Macromolcules* **2008**, *41*, 5928.
(25) Spiro, J. S.; Yang, Y.; Zhang, J. X.; Winnik, M. A.; Rharbi, Y.; Vavasour, J. D.; Whitmore, M.; Jérôme, R *Macromolecules* **2006**, *39*, 7055.
(26) Lindner, P., Zemb, T. Eds. *Neutron, X-rays and Light: Scattering Methods Applied to Soft Condensed Matter*; Elsevier: Amsterdam, 2002Chapter 14.
(27) *Physical Properties of Polymers Handbook*; Mark, J. E., Ed.; American Institute of Physics: New York, 1996.
(28) Doi, M.; Edwards, S. F., *The Theory of Polymer Dynamics*; Clarendon: Oxford, U.K., 1986.
(29) Dhinojwala, A.; Wong, G. K.; Torkelson, J. M. *J. Chem. Phys.* **1994**, *100*, 6047.
(30) Ferry, J. D. *Viscoelestic Properties of Polymers*, 3rd ed.; Wiley: New York, 1980.

MA802734J